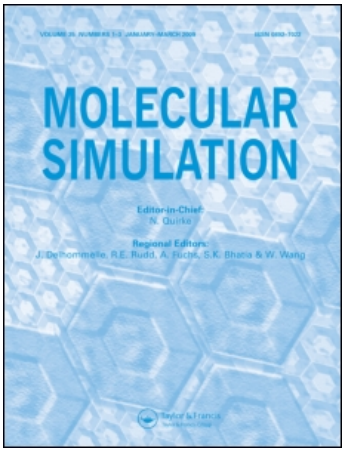

Molecular Simulation
Publication details, including instructions for authors and subscription information:
http://www.informaworld.com/smpp/title~content=t713644482

A computational study of enantioselective adsorption in a homochiral metal-organic framework

Xiaoying Bao[a]; Linda J. Broadbelt[a]; Randall Q. Snurr[a]
[a] Department of Chemical and Biological Engineering, Northwestern University, Evanston, IL, USA

First published on: 21 September 2010

To cite this Article Bao, Xiaoying , Broadbelt, Linda J. and Snurr, Randall Q.(2009) 'A computational study of enantioselective adsorption in a homochiral metal-organic framework', Molecular Simulation, 35: 1, 50 — 59, First published on: 21 September 2010 (iFirst)
To link to this Article: DOI: 10.1080/08927020802422064
URL: http://dx.doi.org/10.1080/08927020802422064

Molecular Simulation
Vol. 35, Nos. 1–2, January–February 2009, 50–59

Taylor & Francis
Taylor & Francis Group

A computational study of enantioselective adsorption in a homochiral metal–organic framework

Xiaoying Bao, Linda J. Broadbelt[1] and Randall Q. Snurr*

Department of Chemical and Biological Engineering, Northwestern University, Evanston, IL, USA

(*Received 14 May 2008; final version received 20 August 2008*)

The potential application of a homochiral metal–organic framework (MOF) made from cadmium corners and BINOL-type linkers for enantioselective separations of chiral hydrocarbons was investigated using grand canonical Monte Carlo simulations. Adsorption of racemic mixtures of (*R*,*S*)-1,3-dimethyl-1,2-propadiene, (*R*,*S*)-1,2-dimethylcyclobutane and (*R*,*S*)-1,2-dimethylcyclopropane was simulated. The results show that an enantiomeric excess (*ee*) of over 50% can be achieved for 1,3-dimethyl-1,2-propadiene, while more moderate *ee* values were observed for the cyclic compounds. The adsorption sites, diastereomeric complexes and adsorption energies were analysed to understand the enantioselective adsorption. It is shown that the small zigzag pores of the homochiral MOF account primarily for the enantioselective adsorption, whereas the larger helical pores show almost no enantioselectivity. The results also demonstrate that both intrinsic enantioselectivity and accessibility of the adsorption sites are important for the overall enantioselective separation.

Keywords: enantioselective adsorption; metal–organic frameworks; GCMC

1. Introduction

The production of enantiopure compounds is essential to the pharmaceutical, food, agricultural and biotechnology industries [1–3]. Chromatography, one of the most important tools for the production of enantiopure compounds, is based on free energy differences of the diastereomeric complexes formed between the enantiomers and the chiral functionalities present on a chiral stationary phase [3–5]. Due to the emergence of new chiral drugs and chemicals, there has been a long standing interest in the development of new chiral stationary phases catering to different separations.

Metal–organic frameworks (MOFs) are a family of microporous, crystalline solids that have attracted much attention in recent years [6–13]. They consist of metal nodes interconnected by organic linkers and are synthesised by self-assembly. Homochiral MOFs with a single sense of chirality throughout their framework are potentially useful as chiral stationary phases for enantioselective separation [14–19]. One major advantage of using homochiral MOFs as chiral stationary phases is their extraordinarily high surface areas, which may enhance the separation rates [14]. In addition, homochiral MOFs can be made from a wide range of metal centres and chiral linkers, and they can be made with various pore sizes and space groups for different enantioselective separation purposes [11,15]. To date, separation of enantiomers using homochiral MOFs has been demonstrated in single-stage equilibration experiments [16–21], often only at a single set of conditions. However, systematic studies of the enantioselective adsorption on homochiral MOFs have not yet been reported.

Wu and Lin [22] recently reported a homochiral MOF $Cd_3L_4(NO_3)_6$, where L is (*R*)-6,6′-dichloro-2,2′-dihydroxy-1,1′-binaphthyl-4,4′-bipyridine. This MOF, which we will refer to as Cd-BINOL, is a colourless crystal and may be useful for enantioselective separations because of its stability and appropriate pore size. Cd-BINOL is stable under prolonged heating at 75°C and is stable upon solvent removal [22]. Cd-BINOL has helical pores of approximate dimension 13.5 × 13.5 Å running in the *c*-direction and zigzag pores of approximate dimension 4.9 × 13.5 Å running in the *a*- and *b*-directions, as shown in Figure 1 [22]. CO_2 adsorption experiments showed that its surface area and pore volume are 772.3 m^2/g and 0.25 cm^3/g, respectively [22]. In this paper, the enantioselective separation capability of Cd-BINOL for three chiral hydrocarbons, namely (*R*,*S*)-1,3-dimethyl-1,2-propadiene (commonly known as 1,3-dimethylallene), (*R*,*S*)-1,2-dimethylcyclobutane and (*R*,*S*)-1,2-dimethylcyclopropane, is presented based on molecular simulations. The competitive adsorption isotherms of the enantiomers of the three sorbates on Cd-BINOL were calculated, and the adsorption sites and the diastereomeric complexes of the three sorbates formed in Cd-BINOL were identified. The importance of both the enantioselectivity and the accessibility of the adsorption sites to enantioseparation will be demonstrated.

*Corresponding author. Email: snurr@northwestern.edu

ISSN 0892-7022 print/ISSN 1029-0435 online

DOI: 10.1080/08927020802422064
http://www.informaworld.com

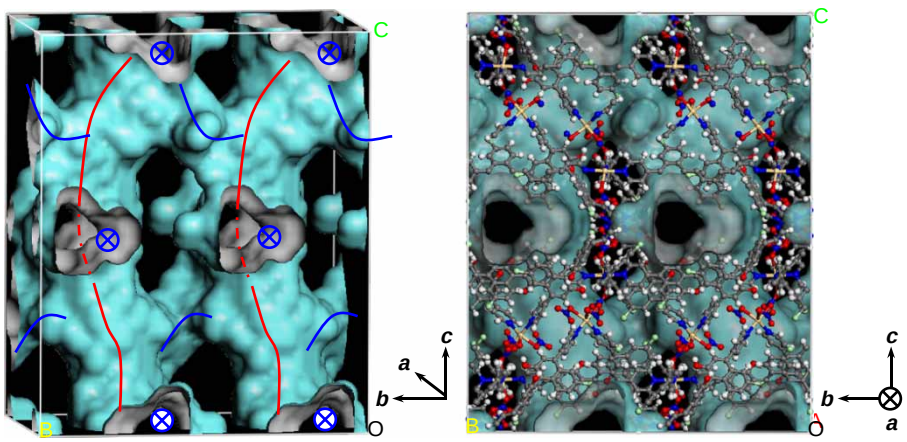

Figure 1. Left: image of the pore structure of the homochiral MOF Cd-BINOL. The pore surfaces shown in cyan (exterior) and grey (interior) were plotted using the Connolly method [29]. The red line follows the helical channel extending in the *c*-direction. The blue line follows the zigzag pores in the *b*-direction. The zigzag pores propagate in the same way in the *a*-direction (marked by blue cross). Right: image of the pore network plus the framework atoms. Grey, C; white, H; green, Cl; blue, N; red, O; yellow, Cd.

2. Methods

Adsorption simulations of racemic mixtures of the sorbates were performed at 300 K with the Music code [23] using the grand canonical Monte Carlo (GCMC) method in the μVT ensemble. Energy-biased insertions of the sorbate molecules were employed to speed up convergence [24]. Acceptance ratios for insertions and deletions were generally above 1% (slightly lower at the higher loadings), which is typically considered high enough for good equilibration in GCMC simulations [24]. The crystallographic information of the Cd-BINOL framework was taken from the literature [22], and the MOF framework was assumed to be rigid. The sorbate molecules were optimised using density functional theory with the B3LYP functional [25] and the 6-31G basis set and were also taken to be rigid during the GCMC simulation. Due to the lack of strongly charged groups in the sorbate molecules, Coulombic interactions were neglected. Dispersion and repulsion interactions were modelled using Lennard-Jones sites on the sorbate and MOF atoms. To further simplify the calculations, the sp^3 CH_3, CH_2 and CH groups in the sorbates were modelled as united atoms. Table 1 lists the Lennard-Jones parameters used for this study. For the MOF, the Lennard-Jones parameters were taken from the universal force field (UFF) [26], while for the sorbates the Lennard-Jones parameters were taken from related studies [5,27,28]. The Lorentz–Berthelot mixing rules were used to obtain the MOF–sorbate interaction parameters. Two hundred and forty million Monte Carlo (MC) moves were attempted during each GCMC simulation.

Simulated annealing using MC in the *NVT* ensemble was employed to identify the energy minima and the diastereomeric complexes. The MC moves employed were translation and rotation. The temperature of the system was cooled from 1500 to 5 K in 12 steps to identify the energy minima of the sorbates within the MOF.

3. Results and discussion

3.1 Adsorption isotherms

The competitive adsorption isotherms, enantiomeric excess (*ee*) and potential energies of the racemic mixtures of (*R*,*S*)-1,3-dimethylallene (DMA) in Cd-BINOL are shown in Figure 2. The enantiomeric excess (*ee*) is defined as the absolute difference between the mole fractions of the two enantiomers. The *R*-enantiomer is favoured, as shown in Figure 2(a) and (b), with *ee* values of ~51% at $f = 0.05$ kPa and ~25% at $f = 1$ kPa. The *ee* decreases with increasing fugacity, which suggests that only certain sites in the pores that are filled at low fugacities are enantioselective to DMA in Cd-BINOL. Figure 2(c) shows

Table 1. Lennard-Jones parameters for the sorbates and Cd-BINOL.

	Atom	ε/*k* (K)	σ (Å)
DMA	CH_3	72.0	3.92
	C	33.2	3.50
	H	15.1	2.50
DMB/DMP	CH_3	98.1	3.77
	CH_2	47.0	3.93
	CH	12.0	4.10
Cd-BINOL	Cl	114.2	3.95
	C	52.8	3.85
	H	22.1	2.89
	O	30.2	3.50
	N	34.7	3.66
	Cd	114.7	2.85

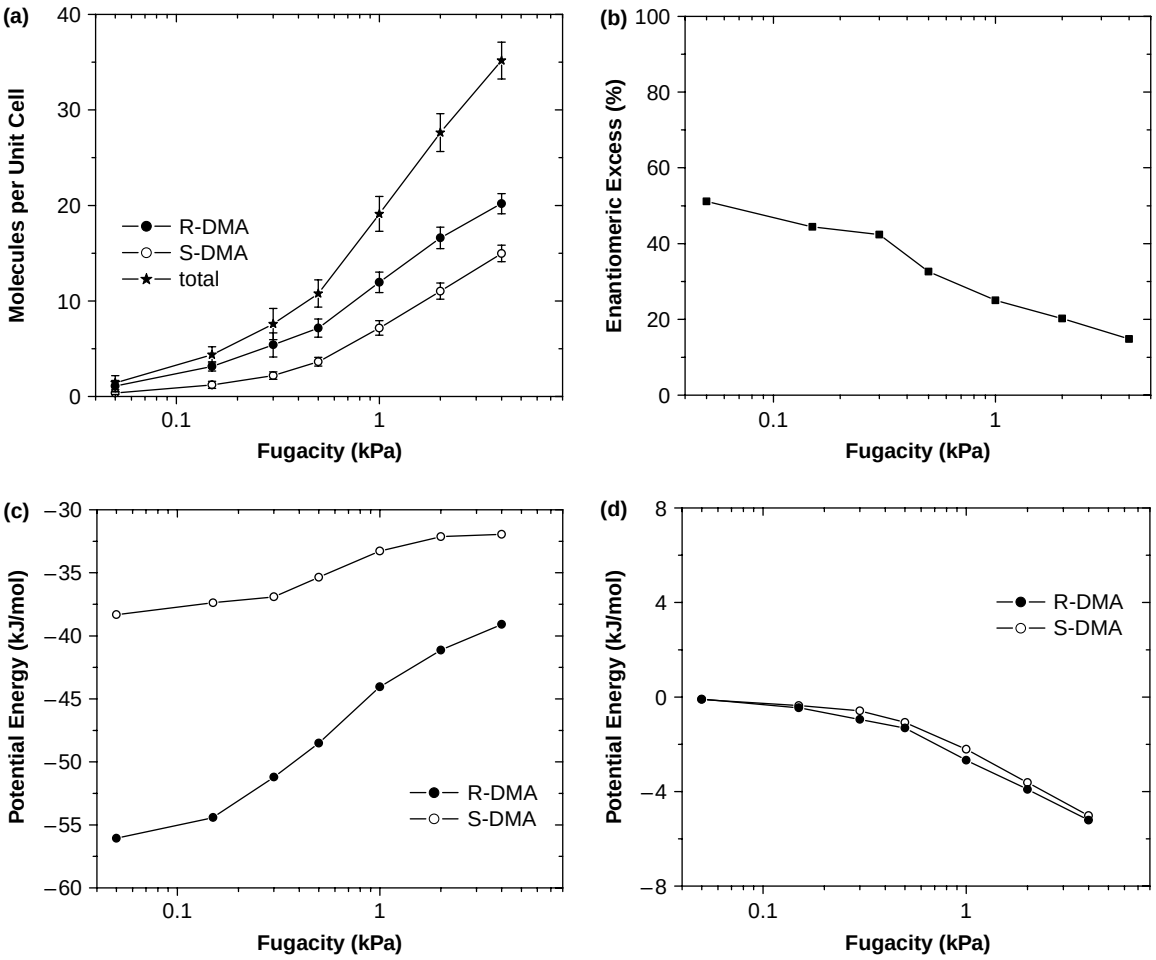

Figure 2. (a) Calculated adsorption isotherms for a racemic mixture of (*R*,*S*)-1,3-dimethylallene (DMA) in Cd-BINOL at 300 K. (b) Enantiomeric excess (*ee*) for selective adsorption of *R*-DMA as a function of fugacity. (c) The interaction energy between DMA and Cd-BINOL per molecule. (d) The sorbate–sorbate interaction energy per molecule.

the interaction energy ΔE between the sorbates and the MOF framework. The marked difference in ΔE (>10 kJ/mol at low fugacities) between the two enantiomers is consistent with the high *ee* at low fugacities, as shown in Figure 2(b). The interaction energy becomes less favourable with increasing loading for both *S*-DMA and *R*-DMA. This is an indication of surface heterogeneity in the MOF: at low loadings, the molecules prefer to occupy the sites with lower energies, while at high loadings less favourable sites are also occupied, causing the interaction energy to become less favourable. Figure 2(d) shows that the interaction energy between the sorbates increases in magnitude with increasing loading, an indication of the attractive lateral interactions between the adsorbed molecules. The sorbate–sorbate interaction energies were almost equal for *R*- and *S*-enantiomers, which indicates that the sorbate–MOF interaction energy difference shown in Figure 2(c) is the key to the enantioselectivity.

Figures 3 and 4 show that for (*R*,*S*)-1,2-dimethylcyclobutane (DMB) and (*R*,*S*)-1,2-dimethylcyclopropane (DMP), respectively, only small *ee* values are observed. While Cd-BINOL selectively adsorbs the *R*-enantiomer of DMA, it is the *S*-enantiomer that is preferred for DMB and DMP. The *ee* values of DMB and DMP increase with fugacity (Figures 3(b) and 4(b)), which is opposite of the trend observed for DMA. This suggests that the enantioselective sites are increasingly filled at higher fugacities. For DMB, the interaction energy ΔE shown in Figure 3(c) shows a maximum with loading for both *R*-DMB and *S*-DMB. The $\Delta(\Delta E)$ is small compared with that of DMA, in agreement with the small *ee*, as shown in Figure 3(b). The initial increase in ΔE is an indication of surface heterogeneity in the MOF, as observed for DMA. The decrease in ΔE at higher loadings is related to the presence of narrow low-energy sites that are filled to only a small extent at low fugacity and are then filled at higher fugacities, as will be shown below. For DMP, ΔE of both

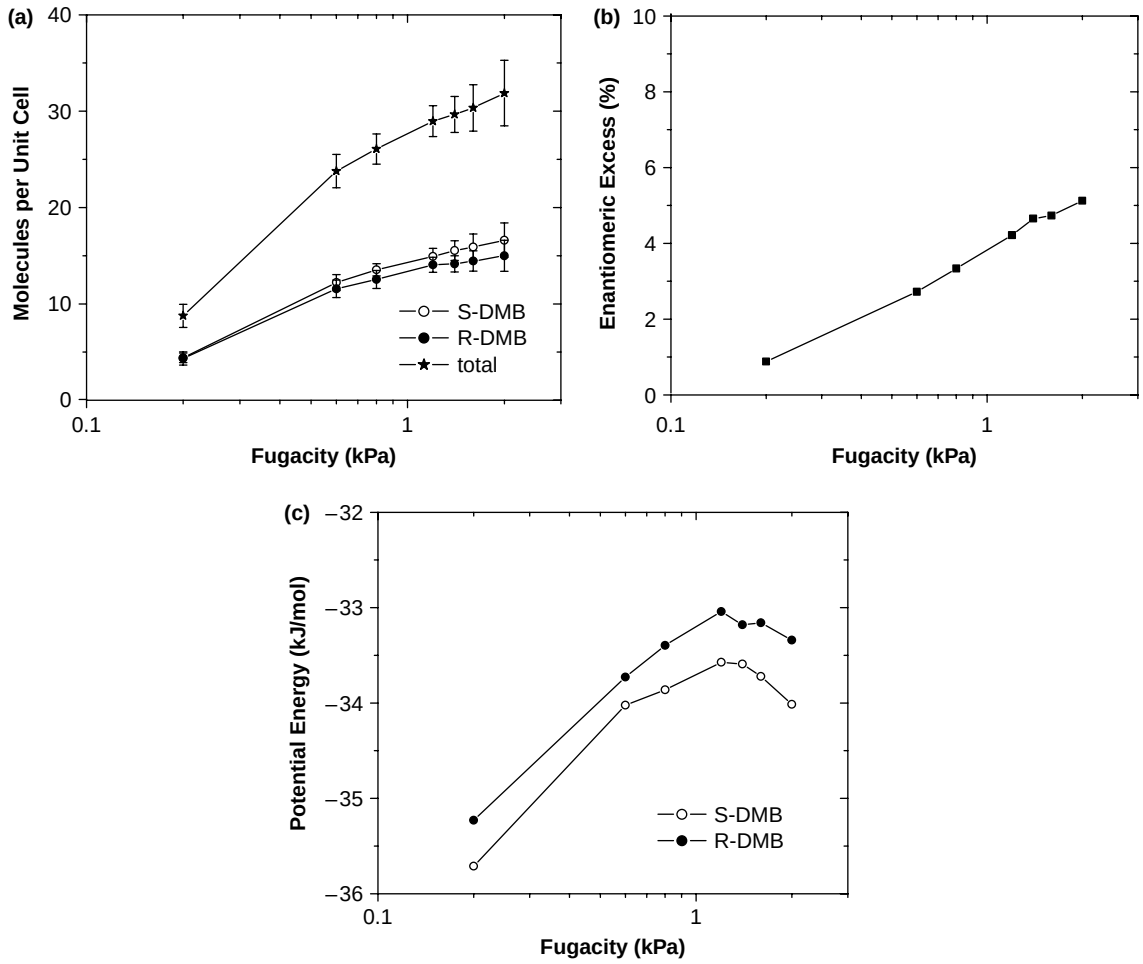

Figure 3. (a) Calculated adsorption isotherms for a racemic mixture of (*R*,*S*)-1,2-dimethylcyclobutane (DMB) in Cd-BINOL at 300 K. (b) Enantiomeric excess (*ee*) for selective adsorption of *S*-DMB as a function of fugacity. (c) The interaction energy between sorbates and Cd-BINOL per molecule.

enantiomers increases with loading (Figure 4(c)). For DMB and DMP, the sorbate–sorbate interaction energies (not shown) are equal for both enantiomers, as observed for DMA.

3.2 Energy minima

Information about the energy minima of the sorbates in the MOF can be useful for the identification of the adsorption sites. The energy minima of the sorbate molecules in the pores of Cd-BINOL were identified using simulated annealing. It should be noted that a large number of energy minima are present on the potential energy surface due to the complexity of the MOF framework. The gradual cooling employed in the simulated annealing procedure tends to identify the deeper and steeper minima on the potential energy surface.

The energy minima for the DMA enantiomers are summarised according to their energies in Table 2. The locations of the minima, represented by balls of various colours, are shown in Figure 5(a). Minima with ΔE greater than -50.7 kJ/mol for *S*-DMA and -46.0 kJ/mol for *R*-DMA are not listed in detail in Table 2, and are all represented by blue balls in Figure 5(a). Four types of sites of adsorption may be classified according to the locations of the minima. Site I is the tip of the zigzag pores where the global minima (shown in red) and a few other lower energy states of the DMA enantiomers are located. Site II is at one side of the helical pores where the low-energy states shown in green are located. Site III is the rest of the helical pore that is opposite to site II, and site IV is the rest of the zigzag pore excluding the tip. The majority of sites II, III and IV are composed of the higher energy states represented by blue balls (Figure 5(a)). An illustration of the four types of adsorption sites is shown in Figure 5(b). The geometric definitions[2] of the four sites are given below. It is interesting that the difference in the ΔE of the global minima of *R*-DMA and *S*-DMA is ~ 9 kJ/mol, which is much larger than what was reported for the adsorption of DMA on chiral metal surfaces [5].

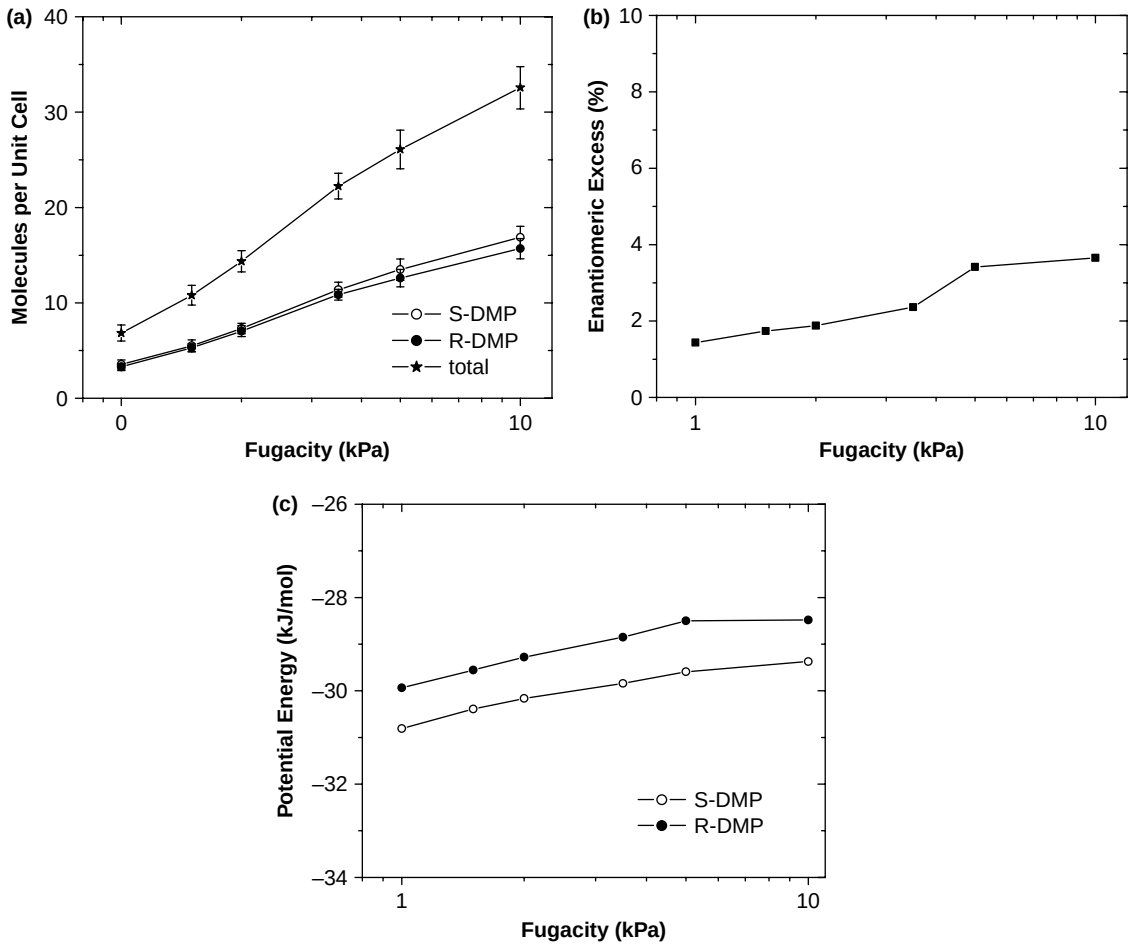

Figure 4. (a) Calculated adsorption isotherms for a racemic mixture of (*R*,*S*)-1,2-dimethylcyclopropane (DMP) in Cd-BINOL at 300 K. (b) Enantiomeric excess (*ee*) for selective adsorption of *S*-DMP as a function of fugacity. (c) The interaction energy between sorbates and Cd-BINOL per molecule.

The energy minima of the DMB and DMP molecules are summarised in Tables 3 and 4, respectively. The global energy minima of the *S*-enantiomers of DMB and DMP are lower than those of the *R*-enantiomers, in agreement with their enantioselectivity. This suggests that the global minima are important in chiral discrimination. The minima for DMB and DMP can be categorised into four adsorption sites in the same way as for DMA.

Table 2. Potential energy minima for (*R*,*S*)-1,3-dimethylallene (DMA).

Colour	*S*-DMA ΔE[a] (kJ/mol)	*R*-DMA ΔE[a] (kJ/mol)
Red	−60.7 (in site I)	−69.9 (in site I)
Orange	−58.6 (in site I)	−58.3 (in site I)
Yellow	−54.9 (in site I)	−56.0 (in site I)
White		−53.0 (in sites I and IV)
Green	−52.4 (in site II)	−49.3 (in site II)
Blue	> −50.7 (in sites II–IV)	> −46.0 (in sites II–IV)

The minima are displayed with the given colours in Figure 5. Sites I–IV are given as a broad classification of the locations of the minima in the MOF framework (see text and Figure 5).

[a] The minima span a narrow range of energies and only the average value is displayed.

3.3 Energy histograms

Energy histograms were calculated showing the fraction of molecules with potential energies in a certain range for each type of site at equilibrium. The energy histograms of the DMA, DMB and DMP molecules in the four types of adsorption sites and the overall pore system are shown in Figures 6, 7 and 8, respectively. Histograms are displayed at both a low and high fugacity for each enantiomer.

For DMA (Figure 6), the relative areas under the histograms of the high-energy sites (sites II–IV) increase substantially at high fugacities, which agrees with the increase in ΔE with fugacity, as shown in Figure 2(c). The area under each histogram curve is related to the number of molecules occupying a particular site. From Figure 6, it can be observed that site I clearly prefers *R*-DMA over

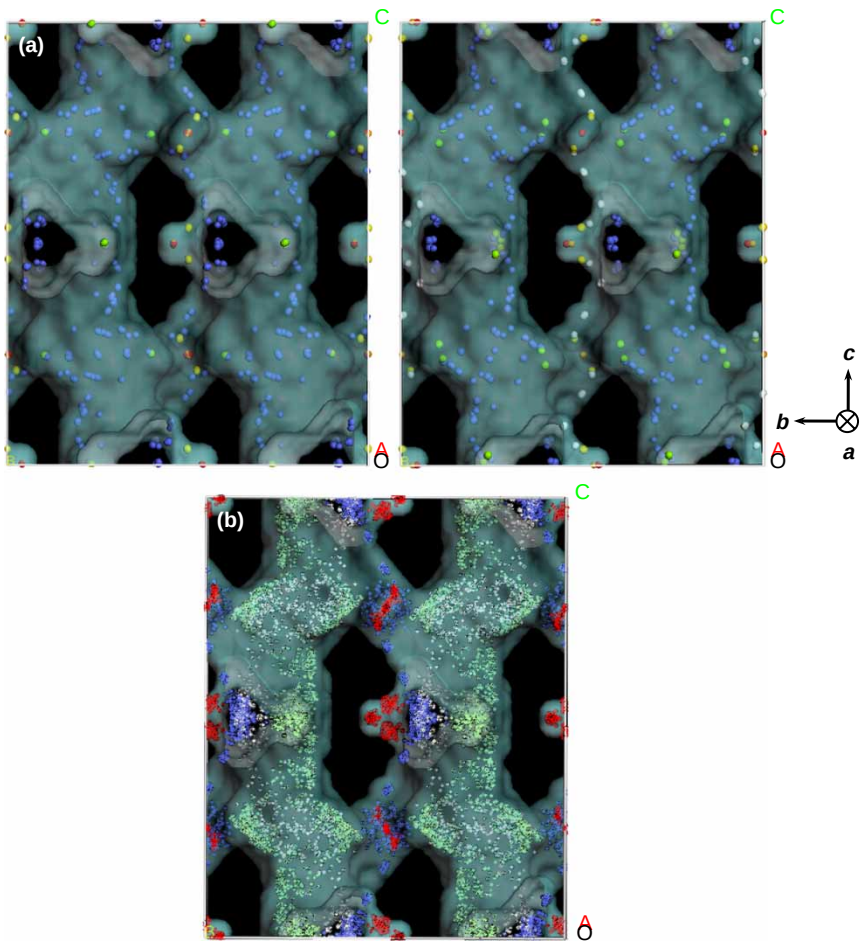

Figure 5. (a) The calculated energy minima of *S*-1,3-dimethylallene (*S*-DMA, left) and *R*-1,3-dimethylallene (*R*-DMA, right) in the pores of Cd-BINOL. The energies and colour scheme of the minima are summarised in Table 2. (b) The positions where the centres of mass of the DMA enantiomers have visited during a period of GCMC simulation colour coded according to adsorption sites. Red, site I; green, site II; white, site III; blue, site IV.

S-DMA, and it is the site that is most enantioselective. Unlike site I, the area under the site II histogram for *S*-DMA is larger than that of *R*-DMA by a small margin. This shows that site II has a slight preference for *S*-DMA. Site IV prefers *R*-DMA; site III, on the other hand, does not show any appreciable enantioselectivity.

One prominent feature of the histograms of DMB and DMP, shown in Figures 7 and 8, respectively, is that site I, although enantioselective to the *S*-enantiomers, is accessible to only a small extent to the sorbate molecules due to steric hindrance. Compared with DMP, the accessibility of site I to DMB is even lower, probably due to the bulkier size of DMB molecules. As fugacity increases, the occupancy of site I increases slightly, which accounts for the increase in *ee* for DMB and DMP at high fugacities shown in Figures 3(b) and 4(b).

Table 3. Potential energy minima for (*R*,*S*)-1,2-dimethylcyclobutane (DMB).

S-DMB ΔE^a (kJ/mol)	*R*-DMB ΔE^a (kJ/mol)
−57.1 (in site I)	−53.1 (in site I)
−52.2 (in site II)	−52.6 (in site II)
−50.2 (in site II)	−49.8 (in site II)
−49.0 (in site II)	−48.2 (in site II)
> −45.2 (in sites II–IV)	> −46.0 (in sites II–IV)

Sites I–IV are categorised in the same way as DMA.
[a]The minima span a narrow range of energies and only the average value is displayed.

Table 4. Potential energy minima for (*R*,*S*)-1,2-dimethylcyclopropane (DMP).

S-DMP ΔE^a (kJ/mol)	*R*-DMP ΔE^a (kJ/mol)
−52.0 (in site I)	−50.9 (in site I)
−44.9 (in site II)	−48.2 (in site I)
−44.2 (in site II)	−46.1 (in site II)
−42.7 (in site II)	−44.3 (in site II)
> −41.7 (in sites II–IV)	> −43.6 (in sites II–IV)

Sites I–IV are categorised in the same way as DMA.
[a]The minima span a narrow range of energies and only the average value is displayed.

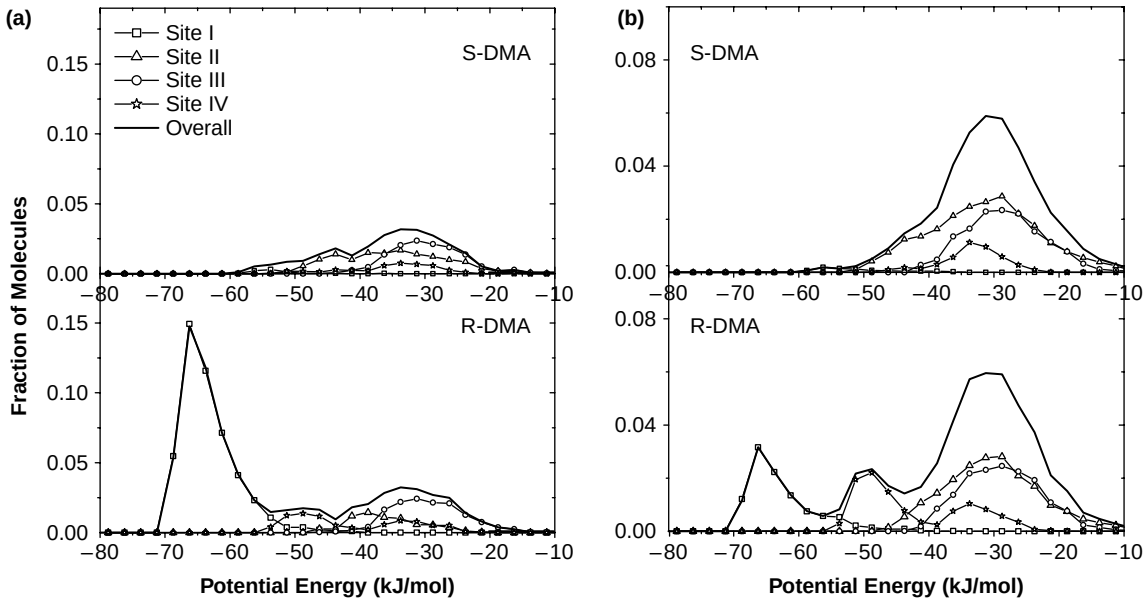

Figure 6. Distribution of energies of individual (*R*,*S*)-1,3-dimethylallene (DMA) molecules in Cd-BINOL at 300 K at (a) $f = 0.2$ kPa and (b) $f = 4$ kPa. The *S*-enantiomer is shown in the top panel, and the *R*-enantiomer is shown in the bottom panel.

3.4 Site occupancies

The number of times that each type of adsorption site was visited by the sorbates at equilibration is complementary to the histograms presented in Figures 6–8. Figure 9 shows that site I is predominantly occupied by *R*-DMA regardless of the fugacity. The enantioselectivity and the high accessibility of site I for DMA explain the high *ee* of the DMA enantiomers at this site. On the other hand, more *S*-DMA is adsorbed at site II than *R*-DMA, but only by a small margin. Little enantioselectivity occurs at site III, while site IV prefers *R*-DMA. The different behaviour of different sites indicates that enantioselective adsorption in a homochiral MOF is an intricate interplay between various sites of adsorption. While some sites favour a certain enantiomer, the other sites may favour another.

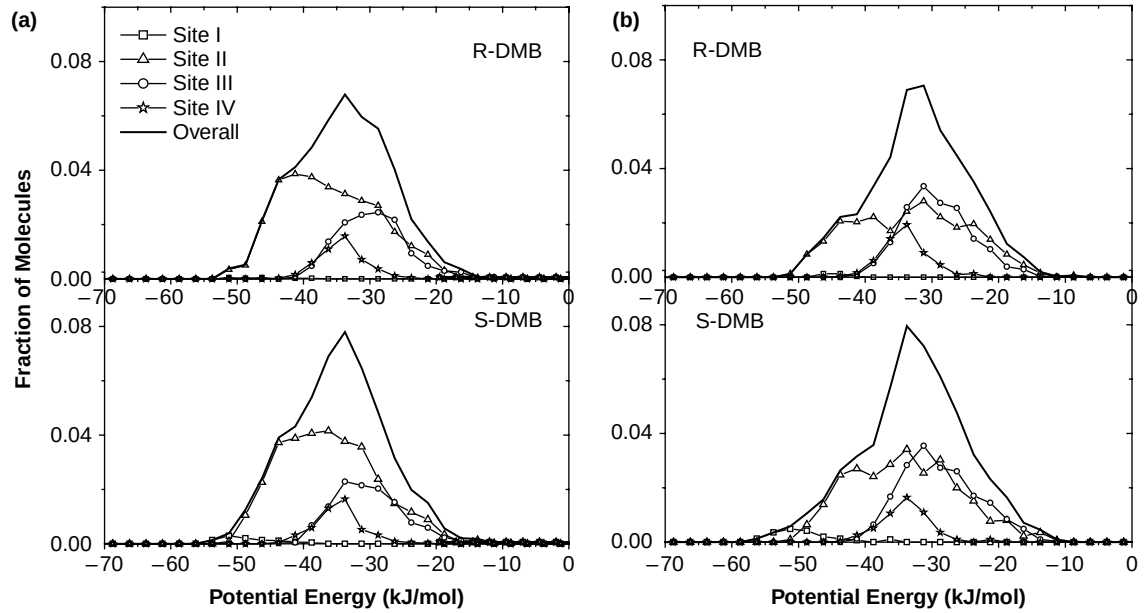

Figure 7. Distribution of energies of individual (*R*,*S*)-1,2-dimethylcyclobutane (DMB) molecules in Cd-BINOL at 300 K at (a) $f = 0.2$ kPa and (b) $f = 2.0$ kPa. The *R*-enantiomer is shown in the top panel, and the *S*-enantiomer is shown in the bottom panel.

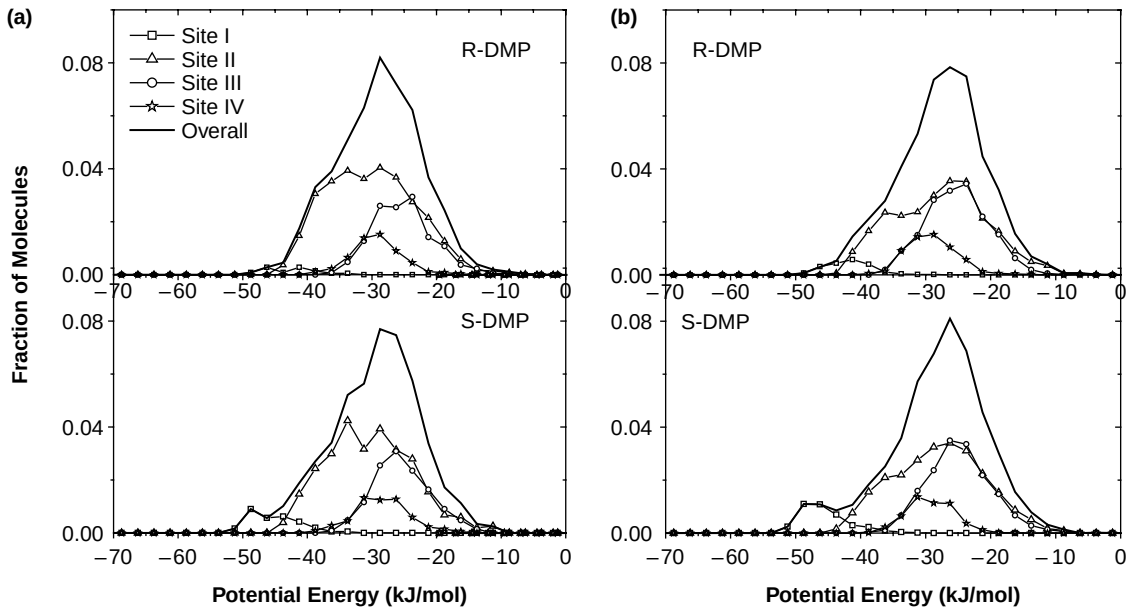

Figure 8. Distribution of energies of individual (*R*,*S*)-1,2-dimethylcyclopropane (DMP) molecules in Cd-BINOL at 300 K at (a) $f = 1$ kPa and (b) $f = 10$ kPa. The *R*-enantiomer is shown in the top panel, and the *S*-enantiomer is shown in the bottom panel.

It is also shown in Figure 9 that when fugacity is increased from 0.15 to 2 kPa, the occupancy of site I for *R*-DMA experiences a 1.5-fold increase, while the occupancies of sites II–IV experience 10- to 20-fold increases. This reinforces the conclusion from Figure 2(c) that at low fugacities, the molecules preferentially occupy the low-energy sites, while at high fugacities, the low-energy sites are essentially filled and more molecules begin to occupy the high-energy sites.

Figure 10 shows that for DMB, sites I–IV all prefer *S*-DMB. While sites II–IV are very weakly enantioselective, site I favours *S*-DMB heavily (inset, Figure 10). For example, at $f = 1.2$ kPa, the ratio of occupancies of *S*-DMB and *R*-DMB in site III is 1.07, while in site I, this ratio is 9.53. Despite its high intrinsic enantioselectivity, site I is accessible to the DMB molecules to only a small extent due to steric hindrance. This explains the small *ee* values observed for the DMB enantiomers in Figure 3(b).

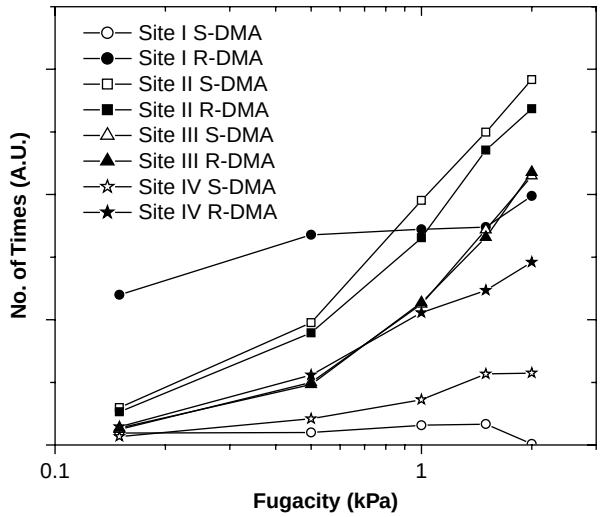

Figure 9. Number of times each type of site was visited by (*R*,*S*)-1,3-dimethylallene (DMA) molecules during a period of a GCMC simulation plotted against fugacity.

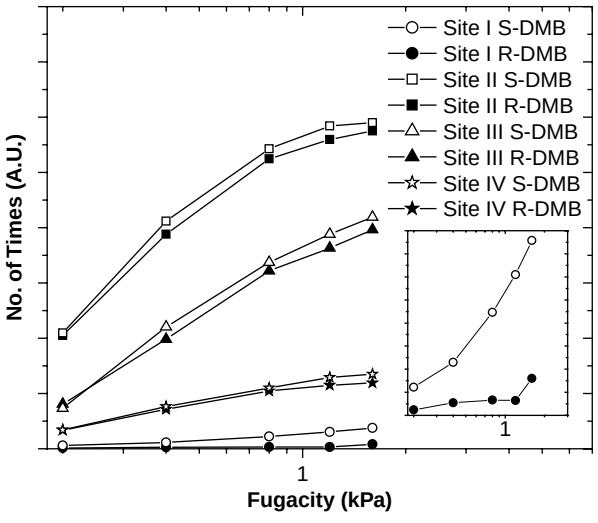

Figure 10. Number of times each type of site was visited by (*R*,*S*)-1,2-dimethylcyclobutane (DMB) molecules during a period of a GCMC simulation plotted against fugacity. The inset shows magnified occupancy information for site I.

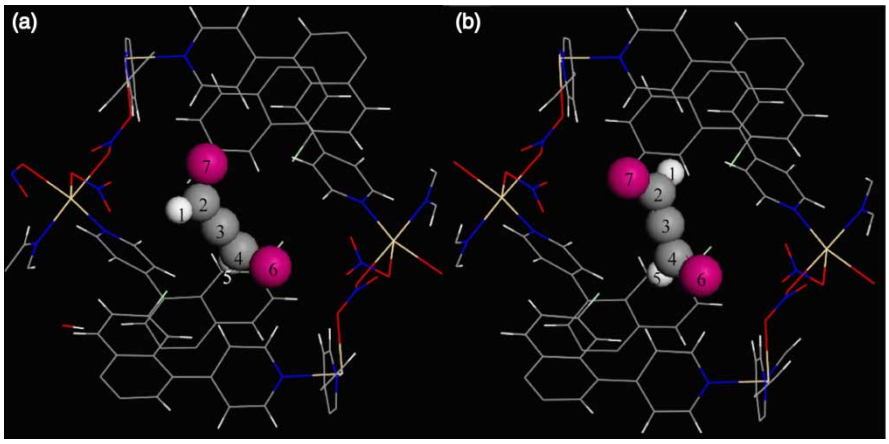

Figure 11. The position and orientation of the (*R*,*S*)-1,3-dimethylallene (DMA) molecules at their global minima for (a) *S*-DMA and (b) *R*-DMA. The MOF atoms within a cut-off of about 9 Å to the centre of mass of the DMA molecules are shown. The DMA molecules are shown as space-filling spheres. In the MOF: C (grey), H (white), Cl (green), N (blue), O (red), Cd (yellow). In DMA: C (grey), H (white), CH_3 (violet red).

It should be noted that unlike DMA, the occupancy of DMB in site I increases faster than the other sites as f increases. For example, when the fugacity is increased from 0.2 to 1.6 kPa, the occupancy of site I for *S*-DMB experiences a sixfold increase, while the occupancy of site II experiences only a 2.5-fold increase. This results in the increase in *ee* at high fugacities, as shown in Figure 3(b). Also, the sharp increase in the occupancy of site I and the low energy of DMB in site I lower the overall ΔE at high fugacities, as shown in Figure 3(c). The results for DMP (not shown) are qualitatively similar to those for DMB, although sites II–IV show no appreciable selectivity.

The energy histograms and site occupancy analysis show that although site I is enantioselective for all three pairs of enantiomers, its ability to be accessed by the three sorbates follows the sequence DMA $\gg$ DMP $>$ DMB. On the other hand, while sites II–IV are easily accessible to all three pairs of enantiomers, they are not strongly enantioselective. Both intrinsic enantioselectivity and accessibility of the adsorption sites are important factors affecting the overall enantioselectivity. For example, only DMA enantiomers with both high enantioselectivity and accessibility to site I demonstrated high *ee* during enantioselective adsorption in the Cd-BINOL MOF. It should be noted that site I lies in the narrow tip of the zigzag pore, whereas site IV lies in the more spacious part of the zigzag pore. Sites II and III, on the other hand, lie in the large helical pore of dimension 13.5 × 13.5 Å. In other words, site I matches the sizes of the sorbates more closely than sites II–IV. This suggests that proper size fitting between the MOF and guest molecules is important for enantioselectivity, but if the fit is too tight it can induce accessibility problems.

Table 5. The potential energy of interaction of each atom (or united atom) in a 1,3-dimethylallene (DMA) molecule shown in Figure 11 with the MOF environment.

No.	Name	*S*-DMA energy (kJ/mol)	*R*-DMA energy (kJ/mol)
1	H	−1.1	−3.1
2	C	−8.2	−10.8
3	C	−8.2	−11.0
4	C	−10.7	−10.9
5	H	−3.0	−3.3
6	CH_3	−15.8	−15.5
7	CH_3	−13.9	−15.5
Total		−61.0	−70.1

3.5 *Diastereomeric complexes*

The analysis above shows that site I, where the global minimum is located, is the most important site for enantioselective adsorption. This is particularly the case for DMA where an energy difference of ~9 kJ/mol was observed between the global minima of the enantiomers. In order to investigate the origin of the energy differences, the diastereomeric complexes formed at the global minima for both *S*-DMA and *R*-DMA are shown in Figure 11. The energy of interaction between each atom (or united atom) in the DMA molecule and the MOF environment is summarised in Table 5.

From Figure 11 and Table 5, it can be observed that atoms 4, 5 and 6 of both enantiomers interact similarly with the MOF framework. However, atoms 1, 2, 3 and 7 of *R*-DMA are able to fit into the MOF framework better than *S*-DMA does. The atoms in Cd-BINOL interacting most strongly with the enantiomers of DMA are mostly the C, H and Cl atoms in the BINOL linker. The DMA molecules interact with more than one nearby chiral linker, which is the key to the large energy difference between the two

diastereomeric complexes.[3] Proper size fitting between the framework and the sorbate molecule leads to the sorbate molecule interacting with multiple linkers, which explains why size fitting is important to enantioselectivity. Further study of the synergistic effect of these chiral linkers is in progress.

4. Conclusion

The potential use of a homochiral MOF, Cd-BINOL, for the enantioselective separation of three chiral hydrocarbons, namely (*R*,*S*)-1,3-dimethylallene (DMA), (*R*,*S*)-1,2-dimethylcyclobutane (DMB) and (*R*,*S*)-1,2-dimethylcyclopropane (DMP), has been demonstrated using molecular simulation. An enantiomeric excess of ~50% can be achieved for the adsorption of a DMA racemic mixture. Site I, located at the tips of the zigzag pores of Cd-BINOL, accounts for most of the enantioselective separation for the three sorbates. Both the intrinsic enantioselectivity of site I and its accessibility are important for overall enantioselective separation. While DMA molecules are able to fit into site I easily and achieve high *ee*, DMB and DMP molecules do not access site I easily, which results in their low *ee* values. It should be noted that while some of the sites in the pore favour the adsorption of one enantiomer, some other sites may favour the adsorption of the other enantiomer. Finally, this study suggests that homochiral MOFs can serve as highly potent chiral separation hosts by exploiting interactions of guest molecules with multiple chiral linkers.

Acknowledgements

We thank the National Science Foundation (CTS-0507013) for financial support. We also thank TeraGrid for the computational resources under project no. TG-CTS080016N.

Notes

1. Email: broadbelt@northwestern.edu
2. Site I: (*x*: −0.068 to 0.103; *y*: 0.000 to 0.073; *z*: 0.243 to 0.300); Site II: (*x*: 0.132 to 0.868; *y*: 0.371 to 0.675; *z*: 0.371 to 0.629); Site III: (*x*: 0.132 to 0.868; *y*: 0.675 to 0.847; *z*: 0.371 to 0.629); Site IV: (*x*: 0.000 to 0.120; *y*: 0.702 to 0.934; *z*: 0.410 to 0.601). Other equivalent locations in the unit cell can be obtained by symmetry.
3. Unpublished result.

References

[1] J.E. Rekoske, *Chiral separations*, AIChE J. 47 (2001), pp. 2–5.
[2] A.M. Rouhi, *Chiral chemistry*, Chem. Eng. News 82 (2004), pp. 47–62.
[3] S. Ahuja, *Chiral Separations by Chromatography*, Oxford University Press, New York, NY, 2000.
[4] G. Guiochon, S. Golshan-shirazi, and A.M. Katti, *Fundamentals of Preparative and Nonlinear Chromatography*, Academic Press, Boston, 1994.
[5] D.S. Sholl, *Adsorption of chiral hydrocarbons on chiral platinum surfaces*, Langmuir 14 (1998), pp. 862–867.
[6] S.R. Batten and R. Robson, *Interpenetrating nets: ordered, periodic entanglement*, Angew. Chem. Int. Ed. 37 (1998), pp. 1460–1494.
[7] M. Eddaoudi, D.B. Moler, H.L. Li, B.L. Chen, T.M. Reineke, M. O'Keeffe, and O.M. Yaghi, *Modular chemistry: secondary building units as a basis for the design of highly porous and robust metal-organic carboxylate frameworks*, Acc. Chem. Res. 34 (2001), pp. 319–330.
[8] S. Kitagawa, R. Kitaura, and S. Noro, *Functional porous coordination polymers*, Angew. Chem. Int. Ed. 43 (2004), pp. 2334–2375.
[9] J.L.C. Rowsell and O.M. Yaghi, *Metal-organic frameworks: A new class of porous materials*, Microporous Mesoporous Mater. 73 (2004), pp. 3–14.
[10] K. Uemura, R. Matsuda, and S. Kitagawa, *Flexible microporous coordination polymers*, J. Solid State Chem. 178 (2005), pp. 2420–2429.
[11] D. Maspoch, D. Ruiz-Molina, and J. Veciana, *Old materials with new tricks: Multifunctional open-framework materials*, Chem. Soc. Rev. 36 (2007), pp. 770–818.
[12] G. Ferey, *Hybrid porous solids: past, present, future*, Chem. Soc. Rev. 37 (2008), pp. 191–214.
[13] R.Q. Snurr, J.T. Hupp, and S.T. Nguyen, *Prospects for nanoporous metal-organic materials in advanced separations processes*, AIChE J. 50 (2004), pp. 1090–1095.
[14] B. McCulloch, P.K. Nicki, and T.A. Brandvold, *Use of small pore silicas as a support for a chiral stationary phase*, US patent 5889180 (1999).
[15] W.B. Lin, *Metal-organic frameworks for asymmetric catalysis and chiral separations*, MRS Bull. 32 (2007), pp. 544–548.
[16] D. Bradshaw, T.J. Prior, E.J. Cussen, J.B. Claridge, and M.J. Rosseinsky, *Permanent microporosity and enantioselective sorption in a chiral open framework*, J. Am. Chem. Soc. 126 (2004), pp. 6106–6114.
[17] D.N. Dybtsev, A.L. Nuzhdin, H. Chun, K.P. Bryliakov, E.P. Talsi, V.P. Fedin, and K. Kim, *A homochiral metal-organic material with permanent porosity, enantioselective sorption properties, and catalytic activity*, Angew. Chem. Int. Ed. 45 (2006), pp. 916–920.
[18] J.S. Seo, D. Whang, H. Lee, S.I. Jun, J. Oh, Y. Jeon, and K. Kim, *A homochiral metal-organic porous material for enantioselective separation and catalysis*, Nature 404 (2000), pp. 982–986.
[19] R. Vaidhyanathan, D. Bradshaw, J.N. Rebilly, J.P. Barrio, J.A. Gould, N.G. Berry, and M.J. Rosseinsky, *A family of nanoporous materials based on an amino acid backbone*, Angew. Chem. Int. Ed. 45 (2006), pp. 6495–6499.
[20] C.D. Wu and W.B. Lin, *A chiral porous 3D metal-organic framework with an unprecedented 4-connected network topology*, Chem. Comm. (2005), pp. 3673–3675.
[21] R.G. Xiong, X.Z. You, B.F. Abrahams, Z.L. Xue, and C.M. Che, *Enantioseparation of racemic organic molecules by a zeolite analogue*, Angew. Chem. Int. Ed. 40 (2001), pp. 4422–4425.
[22] C.D. Wu and W.B. Lin, *Heterogeneous asymmetric catalysis with homochiral metal-organic frameworks: network-structure-dependent catalytic activity*, Angew. Chem. Int. Ed. 46 (2007), pp. 1075–1078.
[23] A. Gupta, S. Chempath, M.J. Sanborn, L.A. Clark, and R.Q. Snurr, *Object-oriented programming paradigms for molecular modeling*, Mol. Simul. 29 (2003), pp. 29–46.
[24] R.Q. Snurr, A.T. Bell, and D.N. Theodorou, *Prediction of adsorption of aromatic hydrocarbons in silicalite from grand canonical Monte-Carlo simulations with biased insertions*, J. Phys. Chem. 97 (1993), pp. 13742–13752.
[25] A.D. Becke, *Density-functional thermochemistry. 3. The role of exact exchange*, J. Chem. Phys. 98 (1993), pp. 5648–5652.
[26] A.K. Rappe, C.J. Casewit, K.S. Colwell, W.A. Goddard, and W.M. Skiff, *UFF, a full periodic table force field for molecular mechanics and molecular dynamics simulations*, J. Am. Chem. Soc. 114 (1992), pp. 10024–10035.
[27] P. Szabelski and D.S. Sholl, *Chiral separation on a model adsorbent with periodic surface heterogeneity*, J. Chem. Phys. 126 (2007), p. 144709.
[28] L.A. Clark, S. Chempath, and R.Q. Snurr, *Simulated adsorption properties and synthesis prospects of homochiral porous solids based on their heterochiral analogs*, Langmuir 21 (2005), pp. 2267–2272.
[29] M.L. Connolly, *The molecular-surface package*, J. Mol. Graphics 11 (1993), pp. 139–143.